Radiation Physics and Chemistry 151 (2018) 36–41

Contents lists available at ScienceDirect

Radiation Physics and Chemistry

journal homepage: www.elsevier.com/locate/radphyschem

Monte Carlo dosimetric evaluation in PET exams for patients with different BMI and heights

Walmir Belinato[a,b], Rogério M.V. Silva[c], Ana P. Perini[a,d,e,f], Lucio P. Neves[a,d,f], Carla J. Santos[a,f], Divanizia N. Souza[g], William S. Santos[a,d,*]

[a] Ionizing Radiation Dosimetry in Medicine Group, Brazil
[b] Departamento de Ensino, Instituto Federal de Educação, Ciência e Tecnologia da Bahia, Vitória da Conquista, BA, Brazil
[c] Instituto do Câncer do Ceará, Fortaleza, CE, Brazil
[d] Instituto de Física, Universidade Federal de Uberlândia, Uberlândia, MG, Brazil
[e] Instituto de Pesquisas Energéticas e Nucleares, Comissão Nacional de Energia Nuclear (IPEN-CNEN/SP), São Paulo, SP, Brazil
[f] Programa de Pós-Graduação em Engenharia Biomédica, Faculdade de Engenharia Elétrica, Universidade Federal de Uberlândia, MG, Brazil
[g] Departamento de Física, Universidade Federal de Sergipe-UFS, São Cristóvão, Sergipe, Brazil

ARTICLE INFO

Keywords:
Monte Carlo simulation
PET
S value
Internal dosimetry

ABSTRACT

In recent years, positron emission tomography (PET), associated with multi-detector computed tomography (MDCT), has become a diagnostic technique widely disseminated to evaluate various malignant tumors and other diseases. However, during PET/CT examinations, the doses of ionizing radiation experienced by the internal organs of the patients due to ^{18}F are unknown, and may be substantial. The aim of this study was to determine a set of S values derived from the ^{18}F-FDG and to use them to determine the absorbed and effective doses of 8 different virtual anthropomorphic phantoms (4 of each gender). These phantoms have different Body Mass Index (BMI), to represent different anatomical characteristics of patients examined in PET. The results of the S values were calculated using the MCNPX (2.7.0) Monte Carlo code. These results were compared to the ICRP 106 reference values, obtained with mathematical anthropomorphic phantoms (MIRD model). Our results of the S values were higher than those obtained and presented at the ICRP 106, mainly due to the differences between the phantoms. The differences between the relative distances of the organs and the chemical and physical characteristics of the phantoms used in this study, in relation to mathematical model, reflected the use of a detailed set of phantoms. Therefore, the results presented in this study provide accurate and reliable data for internal dose calculations for patients undergoing PET examinations.

1. Introduction

Qualitative and quantitative metabolic information are essential for the diagnosis and monitoring of cancer evolution. In this scenario, positron emission tomography (PET) has been invaluable for providing such information (Kapoor et al., 2004). The union of the PET technique with multidetector computed tomography (MDCT), called PET/CT, has allowed the combination of anatomical and metabolic imaging of regions containing positron-emitting isotopes. However, during PET/CT examinations, the doses of ionizing radiation experienced by the internal organs of patients may be substantial, and as it is well known, exposure to ionizing radiation increases the risk of radiation-induced cancer, particularly in younger patients (Huang et al., 2009; Belinato et al., 2017). In PET procedures, the clinical image quantification is performed routinely using the standardized uptake value; this is a non-dimensional unit defined as the activity as imaged by a PET scanner (Sanchez-Crespo, 2013).

Following the rapid growth in the number of procedures in PET/CT, there is an increased concern on the radiation doses from these procedures, as well as a better knowledge of the consequences that ionizing radiation may cause in exposed individuals. In this sense, it is crucial to present new methods for estimating the radiation doses. An alternative, presented in this study, is the use of Monte Carlo method, and a set of mesh virtual anthropomorphic phantoms, to evaluate the radiation doses involved in PET procedures.

In this sense, many research groups have studied new methodologies to establish a standard for calculations of radiation doses in internal organs of patients, undergoing nuclear medicine procedures. In

* Corresponding author at: Ionizing Radiation Dosimetry in Medicine Group, Brazil.
E-mail addresses: wbfisica@gmail.com (W. Belinato), rmv.fisica@gmail.com (R.M.V. Silva), anapaula.perini@ufu.br (A.P. Perini), lucio.neves@ufu.br (L.P. Neves), carlaafro@yahoo.com.br (C.J. Santos), divanizi@ufs.br (D.N. Souza), william@ufu.br (W.S. Santos).

https://doi.org/10.1016/j.radphyschem.2018.05.011
Received 24 June 2017; Received in revised form 11 May 2018; Accepted 14 May 2018
Available online 17 May 2018
0969-806X/

Table 1
Main characteristics of the female and male virtual anthropomorphic phantoms employed in this study Cassola et al. (2010, 2011).

Phantoms	Mass and height percentage	Mass (kg)	Height (cm)	Matrix (columns × lines × slices)	BMI (kg/m^2)	Voxel size (mm^3)
Male	M10_H10	59.3	167.3	238 × 129 × 697	21.2	
	M50_H50	79.0	176.4	239 × 129 × 734	25.4	
	M90_H90	108.5	185.6	298 × 148 × 773	31.5	
Reference Male	MASH3	73.0	176.0	239 × 129 × 731	23.6	2.4 × 2.4 × 2.4
Female	M10_H10	48.6	155.5	219 × 124 × 648	20.1	
	M50_H50	65.0	163.8	221 × 128 × 680	24.2	
	M90_H90	94.0	172.2	271 × 141 × 718	31.7	
Reference Female	FASH3	60.0	163.0	221 × 128 × 677	22.7	

this context, we emphasize the Committee on Medical Internal Radiation Dose (MIRD) which provides a systematic approach to the determination of internal doses, calculated with Monte Carlo simulation and mathematical anthropomorphic phantoms (MIRD model) (Bolch et al., 2008). Although this model constitutes a great advance in the representation of the human anatomy, it still has some limitations, as in the number of organs, as well as their distribution, location, size and chemical and physical composition.

More recently, several researchers have been developing anthropomorphic phantoms based on atlases of the human body, with human anatomy modeling programs, as Blender (2017), MakeHuman (2017), ImageJ (Ferreira and Rasband (2012)). Through the use of these programs, it is possible to construct phantoms with different types of BMI, gender, posture, size, shape and location of the organ and age, maintaining anatomical precision (Cassola et al., 2010, 2011; Lee et al., 2007a, 2007b). These phantoms provide a powerful tool to represent the human anatomy information in a precise way.

Studies show that overweight and obesity have increased dramatically in the world since 1990 (Onis et al., 2010). Particularly in the US, one third of adults and around 17% of children have obesity (Ogden et al., 2014). Considering that PET scans can reach a considerable number of obese adults, this study aims to determine the S values in 8 anthropomorphic phantoms with different gender, BMI and heights. The PET dose contributions are due to the [^{18}F]Fluoro-2-deoxy-2-D-glucose (^{18}F-FDG) radionuclide absorbed in internal organs.

A novelty of this study is the use of a set of adult virtual anthropomorphic phantoms to represent patients of different BMI and heights, involved in PET examinations. In addition to specific patients, we used adult male and female reference anthropomorphic phantoms (MASH3/FASH3), which were constructed based on the anthropometric characteristics of the reference man and woman of the International Commission on Radiological Protection ICRP (2002). We used anthropomorphic phantoms with BMI lower (M10_H10) and higher (M50_H50, M90_H90) than the reference phantoms. In this way, we believe that our results cover a significant portion of patients who undergo PET examinations.

The dosimetric results of this study were compared with the results of the ICRP (2008), which present a set of estimated S values obtained with mathematical anthropomorphic phantoms. Differently from the ICRP (2008), which presents effective dose values calculated based on tissue weighting factors from ICRP (1990), this study presents effective dose values calculated on the basis of tissue weighting factors from ICRP (2007), which are the most recent.

In applications involving the interaction of radiation with matter, the MCNPX code allows the simulation of the interaction of radiation with several types of materials; it is also a useful tool for radiation shielding simulations. This software was developed by the Los Alamos National Laboratory (LANL), US, and it is capable of simulate photon interactions, considering electrons or coupled electrons/photons, among other types of particles and interactions (Pelowitz, 2011). These characteristics made this code very suitable for internal dosimetry, as in PET procedures.

Therefore, in this study, the Monte Carlo N-Particle eXtended (MCNPX version 2.7.0) (Pelowitz, 2011), and the mesh computational anthropomorphic phantoms, were used to determine a set of S values, effective and absorbed doses, for several organs and tissues, with dosimetric importance.

2. Materials and methods

2.1. Male and female adult virtual anthropomorphic phantoms

To represent the patient, four male virtual adult anthropomorphic phantoms, named MASH3, and four female phantoms, named FASH3, were employed. These phantoms were developed by the *Computational Dosimetry Group* from the *Departamento de Energia Nuclear/Universidade Federal de Pernambuco* (DEN/UFPE), using mesh surfaces and polygons (Cassola et al., 2010, 2011, 2013). Their characteristics follow the anatomical and physiological data for the ICRP (2002) reference male and female. These phantoms have all organs and tissues with dosimetric significance, as recommended by the ICRP (2007). The phantoms are produced with mesh surface, and, therefore, must be voxelized to be incorporated in the MCNP Code.

The main anthropometric characteristics, matrix size and voxel size are listed in Table 1, and they are also depicted in Fig. 1. The virtual anthropomorphic phantoms were implemented in the MCNPX (2.7.0) radiation transport code.

One of the main advantages of these phantoms is that they were developed in a standing position, allowing a more realistic representation of the patient. The anatomical effects caused by the gravity, as displacement of the internal organs, lungs compression, sagittal diameter reduction, change in the arms and shoulders position, cranial displacement, were all taken into consideration. The results are, therefore, more realistic than those obtained from phantoms on a laying position.

It is important to note that the patient will undertake the examination on a supine position, but will not remain in this position before and after the exams. This periods will comprise a longer time, and therefore, the standing position will better represent the patient.

In this study, the source organs were the brain, heart, lungs, bladder, remainder tissues and liver. These organs were considered as an isotropic source that emits particles in all directions. The beta energy spectrum (Eckerman and Endo, 2008) was used as the radioactive source in the MCNPX code.

2.2. Calculation of the S values from the ^{18}F distributed at the source organs

The residence times were obtained from the reference ICRP (2008) and the activity value (370 MBq), of the ^{18}F-FDG, was employed to determine the absorbed and effective doses. The dose contributions by the radionuclide were modeled in the MCNPX using the MIRD formalism concept (Eckerman and Endo, 2008). The absorbed dose rate per unit activity in the organs and tissues (r_T), due to the radioactive source (r_S), was determined according to Eq. (1):

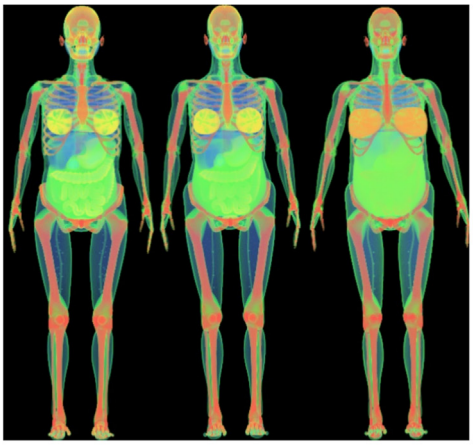

(a) Female M10_H10, M50_H50 and M90_H90 phantoms

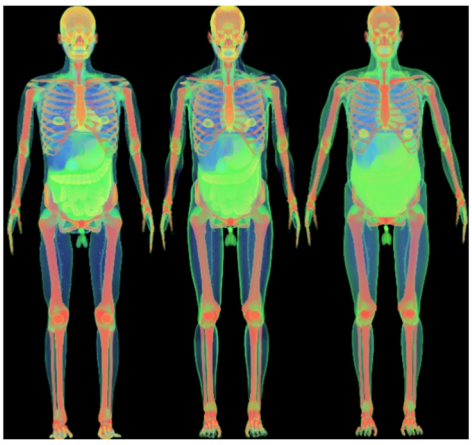

(b) Male M10_H10, M50_H50 and M90_H90 phantoms

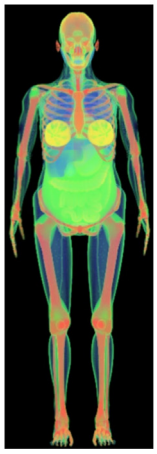

(c) FASH3 phantom

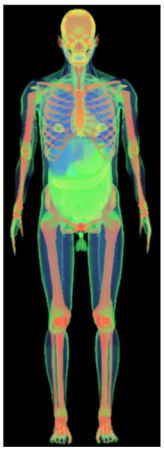

(d) MASH3 phantom

Fig. 1. Front view of the virtual anthropomorphic phantoms (a) female and (b) male, with mass percentage and height of 10, 50 and 90th, used to represent the patient. It also shows the (c) FASH3 and (d) MASH3 reference virtual anthropomorphic phantoms (Cassola et al., 2010, 2011, 2013).

$$\dot{D}(r_T, t) = \sum_{r_S} A(r_S, t) S(r_T \leftarrow r_S, t) \quad (1)$$

where $A(r_S, t)$ is the radionuclide activity in the source, and $S(r_T \leftarrow r_S, t)$ is the S value described in Eq. (2):

$$S(r_T \leftarrow r_S, t) = \sum_i \frac{\Delta_i \phi(r_T \leftarrow r_S, E_i, t)}{M(r_T, t)} \quad (2)$$

where $M(r_T, t)$ is the mass of the organ (kg), Δ_i is the mean energy emitted per nuclear transition and $\phi(r_T \leftarrow r_S, E_i, t)$ is the fraction of the energy absorbed by the organs.

In the present work, the **F8* (MeV/particle) *tally* was employed, considering the energy deposition in the tissues by photons and electrons. The MCNPX default particle physics was used, and the photoelectric effect and the coherent scattering were turned on. We used 1E8 particle histories for the simulations. These values yielded reliable results, with relative uncertainties lower than **5%** (Zaidi, 2006). The uncertainties are of type A, employing a coverage factor of 2.

3. Results and discussion

The S values, as presented in Eq. (1), were employed to the determination of the organ's absorbed doses (D). In Tables 2 and 3 the S values, calculated using the MIRD method associated with PET examinations, are presented. These procedures are usually performed with ^{18}F-FDG, to diagnose or follow the treatment of cancer patients. The activity of 370 MBq was used because it represents an injected activity in patients undergoing PET procedures.

S values were calculated for bone marrow, colon, lung, stomach, remainder tissues, gonads, bladder, oesophagus, liver, thyroid, bone surface, brain, salivary glands, skin and heart. Among these organs, bladder, brain, heart, liver, lung and remainder tissues were considered as source-organs.

Through the S values and residence times of the organs and tissues, provided by the ICRP (2008), it was possible to calculate the absorbed and effective dose values for the 8 virtual anthropomorphic phantoms. These results are also presented in Tables 2, 3 and 5.

From Tables 2 and 3 it is possible to observe that the absorbed doses (mGy), and the S values, are inversely related to phantom's BMI. The main reasons that led to a decrease in dosimetric values when BMI increased were: a BMI increase leads to an increase in adipose tissue around the internal organs, and this providing an additional attenuation material and, consequently, cause a decreasing in dosimetric values of target-organs; anthropomorphic phantoms of lower BMI have

Table 2
S values and absorbed doses for the Male M10_H10, M50_H50, M90_H90 and MASH3 phantoms, considering an activity of 370 MBq. The results were obtained from the total contribution from all source organs (brain, heart, lungs, bladder, remainder tissues and liver).

Organs	MALE: M10_H10		MALE: M50_H50		MALE: M90_H90		MALE: MASH3	
	S value (mGy/MBq.s)	Absorbed Dose (mGy)	S value (mGy/MBq.s)	Absorbed Dose (mGy)	S value (mGy/MBq.s)	Absorbed Dose (mGy)	S value (mGy/MBq.s)	Absorbed Dose (mGy)
Bone marrow	4.7E− 06 (0.01%)	2.7E+ 00 (0.04%)	4.5E− 06 (0.01%)	2.6E+ 00 (0.04%)	4.4E− 06 (0.01%)	2.5E+ 00 (0.03%)	4.5E− 06 (0.01%)	2.6E+ 00 (0.04%)
Colon	6.1E− 06 (0.04%)	4.7E+ 00 (0.28%)	6.0E− 06 (0.03%)	4.7E+ 00 (0.24%)	5.6E− 06 (0.03%)	4.3E+ 00 (0.23%)	5.9E− 06 (0.04%)	4.6E+ 00 (0.27%)
Lung	5.1E− 05 (0.01%)	1.4E+ 01 (0.27%)	5.0E− 05 (0.01%)	1.4E+ 01 (0.27%)	4.2E− 05 (0.01%)	1.2E+ 01 (0.23%)	5.0E− 05 (0.01%)	1.4E+ 01 (0.27%)
Stomach	1.2E− 05 (0.04%)	9.5E+ 00 (0.66%)	1.1E− 05 (0.04%)	9.4E+ 00 (0.65%)	1.0E− 05 (0.04%)	8.7E+ 00 (0.61%)	1.1E− 05 (0.04%)	9.4E+ 00 (0.65%)
Breast	7.0E− 06 (0.19%)	3.0E+ 00 (1.12%)	5.6E− 06 (0.19%)	2.5E+ 00 (0.90%)	3.6E− 06 (0.19%)	1.7E+ 00 (0.60%)	5.7E− 06 (0.19%)	2.5E+ 00 (0.91%)
Remainder tissues	8.0E− 06 (0.01%)	6.6E+ 00 (0.06%)	6.8E− 06 (0.00%)	5.3E+ 00 (0.04%)	6.0E− 06 (0.00%)	4.7E+ 00 (0.04%)	6.7E− 06 (0.00%)	5.2E+ 00 (0.04%)
Gonads	3.0E− 06 (0.17%)	1.7E+ 00 (0.45%)	2.9E− 06 (0.17%)	1.7E+ 00 (0.43%)	2.7E− 06 (0.17%)	1.6E+ 00 (0.41%)	2.9E− 06 (0.17%)	1.7E+ 00 (0.43%)
Bladder	8.1E− 05 (0.03%)	3.4E+ 01 (1.36%)	7.8E− 05 (0.03%)	3.3E+ 01 (1.31%)	7.2E− 05 (0.03%)	3.0E+ 01 (1.14%)	7.8E− 05 (0.03%)	3.3E+ 01 (1.30%)
Oesophagus	1.7E− 05 (0.07%)	7.4E+ 00 (1.03%)	1.8E− 05 (0.07%)	7.9E+ 00 (1.04%)	1.7E− 05 (0.07%)	7.0E+ 00 (0.91%)	1.8E− 05 (0.07%)	7.8E+ 00 (1.03%)
Liver	5.0E− 05 (0.01%)	1.8E+ 01 (0.32%)	4.6E− 05 (0.01%)	1.7E+ 01 (0.30%)	4.1E− 05 (0.01%)	1.5E+ 01 (0.27%)	4.6E− 05 (0.01%)	1.7E+ 01 (0.30%)
Thyroid	6.4E− 06 (0.16%)	5.6E+ 00 (1.40%)	5.8E− 06 (0.17%)	5.0E+ 00 (1.33%)	5.8E− 06 (0.16%)	4.9E+ 00 (1.32%)	5.7E− 06 (0.17%)	4.9E+ 00 (1.31%)
Bone surface	4.7E− 06 (0.01%)	2.7E+ 00 (0.04%)	4.5E− 06 (0.01%)	2.6E+ 00 (0.04%)	4.4E− 06 (0.01%)	2.5E+ 00 (0.03%)	4.5E− 06 (0.01%)	2.6E+ 00 (0.04%)
Brain	4.8E− 05 (0.01%)	1.4E+ 01 (0.16%)	4.7E− 05 (0.01%)	1.4E+ 01 (0.15%)	4.6E− 05 (0.01%)	1.4E+ 01 (0.15%)	4.7E− 05 (0.01%)	1.4E+ 01 (0.15%)
Salivary glands	4.8E− 06 (0.09%)	4.1E+ 00 (0.57%)	4.3E− 06 (0.09%)	3.8E+ 00 (0.54%)	3.9E− 06 (0.09%)	3.5E+ 00 (0.50%)	4.3E− 06 (0.09%)	3.8E+ 00 (0.54%)
Skin	2.4E− 06 (0.02%)	1.4E+ 00 (0.05%)	1.9E− 06 (0.02%)	1.1E+ 00 (0.04%)	1.4E− 06 (0.02%)	8.1E− 01 (0.03%)	2.0E− 06 (0.02%)	1.1E+ 00 (0.04%)
Heart	1.8E− 04 (0.01%)	5.3E+ 01 (1.19%)	1.7E− 04 (0.01%)	5.1E+ 01 (1.15%)	1.6E− 04 (0.01%)	4.8E+ 01 (1.07%)	1.7E− 04 (0.01%)	5.1E+ 01 (1.15%)

Table 3
S values and absorbed doses for the Female M10_H10, M50_H50, M90_H90 and FASH3 phantoms, considering an activity of 370 MBq. The results were obtained from the total contribution from all source organs (brain, heart, lungs, bladder, remainder tissues and liver).

Organs	FEMALE: M10_H10		FEMALE: M50_H50		FEMALE: M90_H90		FEMALE: FASH3	
	S value (mGy/MBq.s)	Absorbed Dose (mGy)	S value (mGy/MBq.s)	Absorbed Dose (mGy)	S value (mGy/MBq.s)	Absorbed Dose (mGy)	S value (mGy/MBq.s)	Absorbed Dose (mGy)
Bone marrow	5.9E− 06 (0.01%)	3.4E+ 00 (0.01%)	5.6E− 06 (0.01%)	3.3E+ 00 (0.01%)	5.3E− 06 (0.01%)	3.1E+ 00 (0.01%)	5.6E− 06 (0.01%)	3.2E+ 00 (0.01%)
Colon	6.7E− 06 (0.04%)	5.7E+ 00 (0.06%)	6.3E− 06 (0.04%)	5.3E+ 00 (0.06%)	5.8E− 06 (0.04%)	5.0E+ 00 (0.06%)	6.3E− 06 (0.04%)	5.4E+ 00 (0.06%)
Lung	6.5E− 05 (0.01%)	1.8E+ 01 (0.02%)	6.2E− 05 (0.01%)	1.7E+ 01 (0.02%)	5.7E− 05 (0.01%)	1.6E+ 01 (0.02%)	6.1E− 05 (0.01%)	1.7E+ 01 (0.02%)
Stomach	1.4E− 05 (0.04%)	1.1E+ 01 (0.07%)	1.4E− 05 (0.04%)	1.1E+ 01 (0.06%)	1.3E− 05 (0.04%)	1.0E+ 01 (0.06%)	1.4E− 05 (0.04%)	1.1E+ 01 (0.07%)
Breast	5.9E− 06 (0.05%)	2.7E+ 00 (0.10%)	6.0E− 06 (0.04%)	2.8E+ 00 (0.08%)	4.4E− 06 (0.04%)	2.1E+ 00 (0.07%)	5.8E− 06 (0.04%)	2.7E+ 00 (0.08%)
Remainder tissues	1.1E− 05 (0.01%)	8.8E+ 00 (0.01%)	9.2E− 06 (0.01%)	7.5E+ 00 (0.01%)	8.3E− 06 (0.01%)	6.7E+ 00 (0.01%)	9.1E− 06 (0.01%)	7.5E+ 00 (0.01%)
Gonads	1.8E− 05 (0.13%)	1.1E+ 01 (0.19%)	1.7E− 05 (0.13%)	9.9E+ 00 (0.20%)	1.6E− 05 (0.13%)	9.6E+ 00 (0.20%)	1.7E− 05 (0.13%)	1.0E+ 01 (0.20%)
Bladder	1.6E− 04 (0.03%)	6.2E+ 01 (0.03%)	1.5E− 04 (0.03%)	5.7E+ 01 (0.03%)	1.4E− 04 (0.03%)	5.2E+ 01 (0.03%)	1.5E− 04 (0.03%)	5.7E+ 01 (0.03%)
Oesophagus	2.3E− 05 (0.07%)	9.5E+ 00 (0.14%)	2.3E− 05 (0.06%)	1.0E+ 01 (0.12%)	1.9E− 05 (0.06%)	8.1E+ 00 (0.13%)	2.3E− 05 (0.07%)	9.6E+ 00 (0.13%)
Liver	6.4E− 05 (0.01%)	2.3E+ 01 (0.02%)	5.6E− 05 (0.01%)	2.1E+ 01 (0.02%)	5.2E− 05 (0.01%)	1.9E+ 01 (0.02%)	5.6E− 05 (0.01%)	2.1E+ 01 (0.02%)
Thyroid	7.5E− 06 (0.16%)	6.4E+ 00 (0.26%)	6.8E− 06 (0.17%)	6.1E+ 00 (0.26%)	6.6E− 06 (0.17%)	5.7E+ 00 (0.27%)	6.5E− 06 (0.17%)	5.7E+ 00 (0.27%)
Bone surface	5.9E− 06 (0.01%)	3.4E+ 00 (0.01%)	5.6E− 06 (0.01%)	3.3E+ 00 (0.01%)	5.3E− 06 (0.01%)	3.1E+ 00 (0.01%)	5.6E− 06 (0.01%)	3.2E+ 00 (0.01%)
Brain	5.3E− 05 (0.01%)	1.6E+ 01 (0.01%)	5.1E− 05 (0.01%)	1.5E+ 01 (0.01%)	5.0E− 05 (0.01%)	1.5E+ 01 (0.01%)	5.1E− 05 (0.01%)	1.5E+ 01 (0.01%)
Salivary glands	5.6E− 06 (0.09%)	4.7E+ 00 (0.14%)	5.1E− 06 (0.09%)	4.4E+ 00 (0.14%)	4.7E− 06 (0.10%)	4.2E+ 00 (0.14%)	5.2E− 06 (0.09%)	4.5E+ 00 (0.14%)
Skin	2.8E− 06 (0.03%)	1.5E+ 00 (0.04%)	2.6E− 06 (0.02%)	1.4E+ 00 (0.04%)	1.9E− 06 (0.02%)	1.0E+ 00 (0.04%)	2.5E− 06 (0.02%)	1.4E+ 00 (0.04%)
Heart	2.4E− 04 (0.01%)	7.2E+ 01 (0.02%)	2.2E− 04 (0.01%)	6.5E+ 01 (0.02%)	2.1E− 04 (0.01%)	6.1E+ 01 (0.02%)	2.2E− 04 (0.01%)	6.5E+ 01 (0.02%)

Table 4
Comparison between absorbed dose per unit of administered activity obtained in our work and the ICRP (2008).

FASH3 (Female)	Absorbed dose per unit of administered activity (mGy/MBq)		
Organs	This study	ICRP (2008)	Difference(%)
Lung	1.39E − 02	2.00E − 02	30%
Remainder tissues	1.69E − 02	1.20E − 02	29%
Bladder	1.38E − 01	1.30E − 01	6%
Liver	2.15E − 02	2.10E − 02	2%
Brain	3.47E − 02	3.80E − 02	9%
Heart	7.62E − 02	6.70E − 02	12%
Effective dose	1.12E − 02	1.09E − 02	2%

less separation between the organs and less adipose tissue along the path between the source organ and target organs, and therefore, reflect an increase in absorbed dose values. In addition, the main cause of the increased absorbed doses of organs from phantoms with low BMI is due to decreased in organ masses.

Besides the natural shielding, caused by the organs and tissues with higher volumes, it is important to note that the energy deposited in the organs did not increase in the same proportion as the mass. The organs with higher doses were the source organs: lung, bladder, liver, heart and brain (self absorbed *S* values).

We also compared the absorbed dose per unit of administered activity from MC simulations and ICRP (2008), and the results are presented in Table 4. In both studies, the results were determined with a reference anthropomorphic phantom representing an female adult. The differences among the S values for effective and equivalent doses are, probably, due to the differences between the phantoms and the method used to determine the S values for effective dose. The values from the ICRP 106 were obtained using a MIRD phantom (174 cm hight, 71 kg body mass, 23.4 kg/m^2). This phantom has tissues and organs represented by only six different materials, while the phantom used in this paper (FASH3, 163 cm hight, 60 kg body mass, 22.7 kg/m^2) has more than 27 different materials.

The substitution of the MIRD model, by a FASH3 model, leaves to an increase of 2% to the S value for effective dose. Furthermore, the S values for effective dose, determined by the ICRP 106, was conducted using the tissue weighting factors (w_T) from ICRP (1990) (reminder tissues - 0.05; bladder - 0.05; liver - 0.05) which were revised and updated in ICRP (2007) (reminder tissues - 0.12; bladder - 0.04; liver - 0.04). As a consequence, all these differences resulted in different S values for the effective dose.

The differences are up to 30% (lung), but one may notice that except for the lungs and remainder tissues, there is a similar trend – a reduction for the S values in the order: liver, brain, heart and bladder. For these organs, the differences are much lower, below 12%. The S values for the lungs (and remainder tissues) are different from those of ICRP 106 mainly due to anatomical structure, since the ICRP 106 used a mathematical phantom, while we used a voxel based phantom. These lead to differences in the size and shape of the organs, such as lungs and remainder tissues (Belinato et al., 2014).

3.1. Effective dose

The organs of the patients who had obtained the highest absorbed dose values in the order of highest to lowest were: heart, bladder, liver, lung, brain, stomach, gonads and remainder tissues. The effective doses for an activity of 370 MBq of ^{18}F-FDG and the type of anthropomorphic phantom are presented in Table 5. Despite the lack of uptake of ^{18}F-FDG in the stomach, this organ received the sixth highest absorbed dose and contributes significantly to the increase in effective dose. This is probably due to the proximity of the lungs, liver and bladder, which were considered source-organs.

Table 5
Effective doses (mSv) for a 370 MBq ^{18}F-FDG activity and the type of anthropomorphic phantom in PET procedures.

Effective doses (mSv)				
M10_H10	M50_H50	M90_H90	MASH3/FASH3	Mean
10 ± 2.5	9.5 ± 2.2	8.6 ± 2.1	9.5 ± 2.2	9.4 ± 2.2

Table 6
Comparison of absorbed dose per unit of administered activity with ^{18}F-FDG distributed in the source-organs.

MASH3 (Male)	Absorbed dose per unit of administered activity (mGy/MBq)		
Organs	This study	Hays et al. (2002)	Difference
Lung	3.8E − 02	1.5E − 02	61%
Remainder tissues	1.4E − 02	1.2E − 02	14%
Bladder	8.9E − 02	7.3E − 02	18%
Liver	4.5E − 02	2.4E − 02	47%
Brain	3.8E − 02	4.6E − 02	17%
Heart	1.4E − 01	6.8E − 02	51%
Mean	6.1E − 02	4.0E − 02	34%

In a study conducted by Quinn et al. (2016) using an average injected activity of 454 MBq, they found an effective dose of (9.0 ± 1.6) mSv (range 3.4–13.6 mSv), which differs by 4% from our results.

The absorbed doses per unit of administered activity, calculated for ^{18}F-FDG, were compared with the literature results (Hays et al., 2002), which were calculated using mathematical anthropomorphic phantoms. As can be seen in Table 6, significant differences were found, reaching over 60% (lung).

The reasons for these differences may be attributed to the anatomical differences between the phantoms. In mathematical anthropomorphic phantoms, organs are represented by mathematical expressions and have many limitations, making it impossible to represent the distance between organs in a more realistic way. The organs and tissues of the mathematical phantoms are composed of a very small number of materials. In addition, they differ in the amount of mass, size and contours of the organs.

Specific absorbed fractions (SAF) are used to estimate radiation doses for radiopharmaceuticals and dose factors (DF), implemented in programs such as MIRDOSE (Stabin, 1996) and OLINDA/EXM code (Stabin et al., 2005). In the literature, studies show that obese adults present a variation in the SAF values of up to 30% for organs within the trunk (Marine et al., 2010; Clark et al., 2010). Thus, the variations of the doses in the trunk organs obtained by this study follows the same pattern, with results predicted in the literature, although the metric used was different.

4. Conclusions

In this study we presented a dosimetric study, which uses Monte Carlo simulation and mesh anthropomorphic phantoms, to determine a set of S values, absorbed and effective doses of organs and tissues during PET procedures. Our results were compared with those from the literature, where mathematical phantoms were employed, and presented significant differences, reaching over 60%. These differences may be justified due to simplifications in the mathematical phantoms. In these phantoms the organs and tissues are represented by mathematical equations, while in our case the organs and tissues are more realistic and they were build using mesh surfaces. The highest values for absorbed doses were to the source organs. Therefore, this work is important to point out the doses involved in PET procedures, considering different BMI, heights and gender.

As expected, the organs with self-absorption (lungs, bladder, liver, brain and heart) were those that acquired the highest values of absorbed doses. The exception was the stomach, probably due to its proximity to the lungs, liver and bladder. In addition, the dosimetric results presented a small dependence with the BMI. Patients of the female gender generally have a lower body mass than those of the male gender and, therefore, they have the most effective dose increase. The minimum, maximum and mean effective dose calculated for an administered activity of 370 MBq were 8.6 ± 2.1 mSv (M90_H90), 10 ± 2.5 mSv (M10_H10) and 9.4 ± 2.2 mSv, respectively. These values are higher than those published by the ICRP 106 (7.0 mSv). The dosimetric results presented by our study showed a strong dependence on the organ mass. Phantoms with lower BMI received higher absorbed doses.

Acknowledgments

The authors would like to thank Dr. Richard Kramer for kindly providing the virtual anthropomorphic phantoms. This work was partially supported by the Brazilian agencies: Fundação de Amparo à Pesquisa do Estado de Minas Gerais (FAPEMIG, Grants No. APQ-03049-15 and APQ-02934-15) and Conselho Nacional de Desenvolvimento Científico e Tecnológico (CNPq, Grants nos. 421603/2016-0, 420699/2016-3 and 168947/2017-0).

References

Belinato, W., Santos, W.S., Silva, R.M.V., Souza, D.N., 2014. Monte Carlo estimation of radiation dose in organs of female and male adult phantoms due to FDG-F18 absorbed in the lungs. EPJ Web Conf. - Int. Nucl. Phys. Conf. 66, 100021–100024.

Belinato, W., Santos, W.S., Perini, A.P., Neves, L.P., Caldas, L.V.E., Souza, D.N., 2017. Estimate of S-values for children due to six positron emitting radionuclides used in PET examinations. Radiat. Phys. Chem. 140 (1), 51–56. http://dx.doi.org/10.1016/j.radphyschem.2017.02.038.

Blender Foundation. Blender free and open source 3D creation suite (2017).URL ⟨https://www.blender.org⟩.

Bolch, W.E., Eckerman, K.F., Sgouros, G., Thomas, S.R., 2008. MIRD Pamphlet No. 21: a generalized schema for radiopharmaceutical dosimetry standardization of nomenclature. J. Nucl. Med. 50 (3), 477–484. http://dx.doi.org/10.2967/jnumed.108.056036.

Cassola, V.F., Lima, V.J.D., Kramer, R., Khoury, H.J., 2010. FASH and MASH: female and male adult human phantoms based on polygon mesh surfaces: i. Development of the anatomy. Phys. Med. Biol. 55 (1), 133–162. http://dx.doi.org/10.1088/0031-9155/55/1/009.

Cassola, V.F., Milian, F.M., Kramer, R., de Oliveira Lira, C.A., Khoury, H.J., 2011. Standing adult human phantoms based on 10th, 50th and 90th mass and height percentiles of male and female Caucasian populations. Phys. Med. Biol. 56 (1), 3749–3772. http://dx.doi.org/10.1088/0031-9155/56/13/002.

Cassola, V.F., Kramer, R., de Melo Lima, V.J., de Oliveira Lira, C.A.B., Khoury, H.J., Vieira, J.W., Brown, K.R., 2013. Development of newborn and 1-year-old reference phantoms based on polygon mesh surfaces. J. Radiol. Prot. 33 (3), 669–691. http://dx.doi.org/10.1088/0952-4746/33/3/669.

Clark, L., Stabin, M., Fernald, M., Brill, A., 2010. Changes in radiation dose with variations in human anatomy: moderately and severely obese adults. J. Nucl. Med. 51 (6), 929–932. http://dx.doi.org/10.2967/jnumed.109.073015.

Eckerman, K.F., Endo, A., (2008). MIRD: Radionuclide Data and Decay Schemes, 2nd Edition. The Society of Nuclear Medicine, Reston, VA, CD data.

Ferreira, T., Rasband, W., (2012). ImageJ User Guide. Tech. Rep. ImageJ/Fiji 1.46, ⟨http://imagej.nih.gov/ij/docs/guide⟩.

Hays, M., Watson, E., Thomas, S., Stabin, M., 2002. MIRD dose estimate report no. 19: radiation absorbed dose estimates from (18)F-FDG. J. Nucl. Med. 43 (2), 210–214.

Huang, B., Law, M.W., Khong, P., 2009. Whole-body PET/CT scanning: estimation of radiation dose and cancer risk. Radiology 251 (1), 166–174. http://dx.doi.org/10.1148/radiol.2511081300.

ICRP Publication 60. 1990 Recommendations of the International Commission on Radiological Protection, Ann. ICRP 21 (1–3), 1991.

ICRP Publication 89. Basic Anatomical and Physiological Data for Use in Radiological Protection Reference Values, Ann. ICRP 32 (3–4), 2002.

ICRP Publication 103. The 2007 Recommendations of the International Commission on Radiological Protection, Ann. 37 (2–4), 2007.

ICRP Publication 106. Radiation Dose to Patients from Radiopharmaceuticals. Addendum 3 to ICRP Publication 53, Ann. ICRP 38 (1–2), 2008.

Kapoor, V., McCook, B.M., Torok, F.S., 2004. An introduction to PET-CT imaging. Radiographics 24 (2), 523–543. http://dx.doi.org/10.1148/rg.242025724.

Lee, C., Lee, C., Lodwick, D., Bolch, W., 2007a. NURBS-based 3-D anthropomorphic computational phantoms for radiation dosimetry applications. Radiat. Prot. Dosim. 127 (1–4), 227–232. http://dx.doi.org/10.1093/rpd/ncm277.

Lee, C., Lodwick, D., Hasenauer, D., Williams, J.L., Lee, C., Bolch, W., 2007b. Hybrid computational phantoms of the male and female newborn patient: nurbs-based whole-body models. Phys. Med. Biol. 52 (12), 3309–3333. http://dx.doi.org/10.1088/0031-9155/52/12/001.

MakeHuman Team. MakeHuman™ Open source tool for making 3D characters (2017). URL ⟨http://www.makehuman.org/⟩.

Marine, P., Stabin, M., Fernald, M., Brill, A., 2010. Changes in radiation dose with variations in human anatomy: larger and smaller normal-stature adults. J. Nucl. Med. 51 (5), 806–811. http://dx.doi.org/10.2967/jnumed.109.073007.

Ogden, C.L., Carroll, M.D., Kit, B.K., Flegal, K.M., 2014. Prevalence of childhood and adult obesity in the united states. 2011–2012, JAMA 311 (8), 806–814. http://dx.doi.org/10.1001/jama.2014.732.

Onis, M., Blössner, M., Borghi, E., 2010. Global prevalence and trends of overweight and obesity among preschool children. Am. J. Clin. Nutr. 82 (5), 1257–1264. http://dx.doi.org/10.3945/ajcn.2010.29786.

Pelowitz, D.B., (2011). MCNPX User's Manual. Version 2.7.0, Report LA-CP-11-00438. Los Alamos National Laboratory.

Quinn, B., Dauer, Z., Pandit-Taskar, N., Schoder, H., Dauer, L.T., 2016. Radiation dosimetry of 18F-FDG PET/CT: incorporating exam-specific parameters in dose estimates. BMC Med. Imaging 16 (41), 1–11. http://dx.doi.org/10.1186/s12880-016-0143-y.

Sanchez-Crespo, A., 2013. Comparison of Gallium-68 and Fluorine-18 imaging characteristics in positron emission tomography. Appl. Radiat. Isot. 76, 55–62. http://dx.doi.org/10.1016/j.apradiso.2012.06.034.

Stabin, M.G., Sparks, R.B., Crowe, E., 2005. OLINDA/EXM: the second-generation personal computer software for internal dose assessment in nuclear medicine. J. Nucl. Med. 46 (6), 1023–1027.

Stabin, M.G., 1996. MIRDOSE: personal computer software for internal dose assessment in nuclear medicine. J. Nucl. Med. 37 (3), 538–546.

Zaidi, H., (2006). Monte Carlo modeling in nuclear medicine imaging. In: Zaidi, H. (Ed.), Quantitative Analysis in Nuclear Medicine Imaging, Springer Science + Business Media, New York, NY 10013, USA, Ch. 11, pp. 358–390. http://dx.doi.org/10.1007/b107410.